Journal of Nuclear Materials 433 (2013) 504–513

Contents lists available at SciVerse ScienceDirect

Journal of Nuclear Materials

journal homepage: www.elsevier.com/locate/jnucmat

Effect of the substitution of f-electron elements on the structure and elastic properties of UO_2

Rakesh K. Behera [a,*], Chaitanya S. Deo [a,*], Haixuan Xu [b]

[a] Nuclear and Radiological Engineering Program, George W. Woodruff School of Mechanical Engineering, Georgia Institute of Technology, Atlanta, GA 30332, USA
[b] Materials Science and Technology Division, Oak Ridge National Laboratory, Oak Ridge, TN 37831, USA

ARTICLE INFO

Article history:
Received 19 April 2012
Accepted 25 September 2012
Available online 6 October 2012

ABSTRACT

The chemistry of nuclear reactor fuel initially is complex, and continuous loss of uranium and plutonium, and formation of a broad range of new species due to fission introduce a challenging time-dependence to this chemistry. Lanthanides and/or Actinides substitution on the uranium sublattice occurs (a) during fission, (b) when mixed oxide fuel is used, and (c) when minor Actinides are reprocessed in UO_2 matrix fuel as part of a closed nuclear fuel cycle. These fission products and minor Actinides influence a variety of thermo-physical properties, which depend on structure and elastic properties. How these structural and elastic properties vary with Lanthanide and Actinide substitution is not well studied. In this study we use atomic level simulations to investigate the effect of 4+ and 3+ ion substitutions on the structural and elastic properties of urania matrix. Our results show that most of the 4+ ions reduce the overall lattice parameter, while all the 3+ ions considered here increased the lattice parameter of the urania matrix. This effect is guided by the interplay between the elastic and electrostatic effect of the substituted ions. We calculate the chemical expansion and chemical expansion coefficient with the change in concentration based on the ionic radii of the substituted 3+ and 4+ ions. In general, elastic properties are enhanced for 4+ ions substitution and reduced for 3+ ion substitution.

1. Introduction

The chemistry of nuclear reactor fuel initially is complex, and continuous loss of uranium and plutonium, and formation of a broad range of new species due to fission introduce a challenging time-dependence to this chemistry. The fuel ultimately contains multiple f-electron elements: uranium (U), plutonium (Pu), americium (Am), neptunium (Np), and curium (Cm) as well as many lighter elements. Lanthanides and/or Actinides substitution on the uranium sublattice occurs (a) during fission, (b) when mixed oxide fuel is used, and (c) when minor Actinides are reprocessed in UO_2 matrix fuel as part of a closed nuclear fuel cycle. These are described below.

Fission yield of a uranium based fuel can generate more than 20 fission products [1–3]. These can be classified broadly [1] as (i) fission gases and other volatile products (Br, Kr, I, and Xe); (ii) fission products forming metallic precipitates (from Mo to Te in the periodic table); (iii) fission products forming oxide precipitates; and (iv) fission products dissolved as oxides in the fuel matrix. In addition neutron capture and decay reactions generate minor Actinides such as Ce, Nd, Pm, Sm, Eu, and Gd in the Lanthanide series and Np, Pu, Am, and Cm in the Actinide series. The generation of these fission products and minor Actinides affect the thermo-physical properties of the fuel, mechanical properties, thermal conductivity, ionic diffusion, phase stability. In order to understand the microstructural evolution of nuclear fuel during fabrication and operation, it is essential to understand the effect of these elements on structure and elastic properties of the host UO_2 matrix [4–6].

Mixed oxide fuels represent another situation where Actinides substitute on the uranium sublattice. One very attractive way to reduce the plutonium inventory is to reuse the plutonium as a mixed oxide (MOX) fuel in power reactors [7]. There are different MOX fuels used to reduce the plutonium concentration in the spent fuel [7–9], those are UO_2–PuO_2, UO_2–ThO_2, and PuO_2–ThO_2. While MOX fuels improve the proliferation resistance, a systematic characterization of fundamental properties such as the structural, elastic properties and phase stability is necessary.

Further, closed nuclear fuel cycles often involve the transmutation of minor Actinides in a host matrix [9]. The technologies for incorporating significant amounts of minor oxides into fuel are not well established. There are several minor Actinide fuel or target options available for eventual application in nuclear transmutation systems [9]. In particular minor Actinide rich fuels (MA-MOX) are extremely important for transmutation. The concentrations of minor Actinides in both MOX and MA-MOX range between 20% and 25% cation substitution in the urania matrix.

* Corresponding authors. Tel.: +1 404 894 2823; fax: +1 404 894 3733 (R.K. Behera), tel.: +1 404 385 4928 (C.S. Deo).
E-mail addresses: rakesh.behera@me.gatech.edu (R.K. Behera), chaitanya.deo@me.gatech.edu (C.S. Deo).

0022-3115/$ - see front matter © 2012 Elsevier B.V. All rights reserved.
http://dx.doi.org/10.1016/j.jnucmat.2012.09.031

Quite often Actinide substitution is experimentally studied with Lanthanide surrogates. For example, ceria-based MOX studied by Kim et al. [10] characterized the influence of up to 30% ceria substitution in the urania matrix. The thermal conductivities were calculated from measured thermal diffusivity as a function of the cerium concentration. For the normalization of the thermal conductivities, structure (lattice parameters and theoretical densities) was examined using X-ray diffractometry.

These examples show the need to understand the effect of Lanthanide and Actinide substitution in the uranium sublattice. First-principles calculation based on density functional theory (DFT) is the ideal approach to obtain such fundamental properties. However, first-principles calculation has its internal limitation in describing highly correlated systems such as UO_2. In order to get the correct ground state electronic properties additional parameters (such as the Hubbard correction [11,12]) have to be considered, which is not trivial. For example, using first-principles calculations, Yu et al. [13] have investigated the effect of the Hubbard correction on the defect properties and phase transition in UO_2. In comparison, empirical potentials fit to fundamental properties are available for most relevant Lanthanide and Actinde oxides. Therefore, in this work we use atomistic simulation method with empirical potentials to address the effect of substitution in urania matrix.

Recent work by Middleburg et al. [14] investigated the accommodation of trivalent dopants in stoichimetric and hyper-stoichiometric urania fuel using atomic scale simulations. In particular these researchers have addressed the clustering and solution energies of different 3+ ions, where these trivalent ions help in manipulating the microstructure and the neutronic response of the urania fuel. Even though there has been a lot of work on the solution energies, incorporation energies, structural arrangement and clustering of the 4+ and 3+ ions (Lanthanides and Actinides) in the literature [14,15], there is a limited understanding of the effect of these Lanthanides and Actinides on the structure and elastic properties of the urania matrix with varying Lanthanide and Actinide concentration.

The rest of the article is organized as follows: Section 2 discusses the interatomic potentials and simulation method. The results are reported in Section 3, where all the potentials are used to estimate the properties of pure UO_2. This section discusses the specific case of Ce^{4+} and U^{3+} ions substitution and extends the calculations to include other 4+ and 3+ Lanthanides and Actinides. Section 4 includes the discussion and conclusion section. In Section 4 we have presented the summary of all the ion substitution on chemical expansion and equivalent temperature.

2. Methodology

In this study we have investigated the structural and mechanical properties of UO_2 and substituted urania-systems using atomic level simulations. While the qualitative trends predicted with molecular dynamics (MD) simulation is very useful, the quantitative comparison with experiment depends on the fidelity of the interatomic potentials used to describe the system. Since we are interested in characterizing the structural and elastic properties of UO_2 and substitution of Lanthanides and Actinides in the urania matrix, we have collected potentials which are consistent and transferable.

The ground state phase of UO_2 exhibits the Fluorite structure with Fm $\bar{3}$ m symmetry (space group # 225). In the UO_2 lattice, uranium ions occupy the face centered positions and oxygen ions occupy the tetrahedral sites. In order to simulate urania systems with Lanthanides and Actinides, we have collected a set of interatomic potentials [15–21] where the O–O interactions are the same and transferable between U and other elements of interest. A list of self-consistent interatomic potentials available to describe the Lanthanides and Actinides are listed in Table 1. These potentials can be separated based on the charge definition on each ion. The potentials can be defined as a shell-model or rigid-ion model. In the shell model [22], each ion is described by a core and a shell, the sum of whose charges is the ionic charge of each species. The core and shell on each ion is attached to each other via a spring (which can be harmonic or anharmonic). The interaction between the core and shell of an atom coupled by a harmonic spring is given by:

$$V(\omega) = \frac{1}{2}k_2\omega^2 \tag{1}$$

where ω is the core-shell displacement, and k_2 is the harmonic spring constants. The interatomic potentials with shell-model are Grimes01 [15], Grimes02 [16], Grimes03 [17] and Nadeem [18] referred as Pot1, Pot2, Pot3 and Pot4 respectively from here in after. Pot1 can describe U^{4+}, and Ce^{4+}, while Pot2 provides consistent parameters for U^{4+}, Pu^{4+}, Ce^{4+}, Ce^{3+}, Sm^{3+}, and Gd^{3+}. Pot3 is the only potential that can describe the most 3+ ion descriptions and includes consistent parameters to describe U^{4+}, U^{3+}, Pu^{4+}, Pu^{3+}, Nd^{3+}, Sm^{3+}, Eu^{3+}, and Gd^{3+}. Pot4 can describe systems with Th^{4+}, U^{4+}, and Ce^{4+}. There are two rigid ion models, where the ions are defined by point charges. The Osaka potential (Pot5) [19] can describe most of the Actinides (Th^{4+}, U^{4+}, Np^{4+}, Pu^{4+}, and Am^{4+}) and Gd^{3+} consistently; while Uchida potential (Pot6) [20,21] has self-consistent parameters to describe a few Actinides (Th^{4+}, U^{4+}, Am^{4+}, and Am^{3+}) of interest.

In order to simulate the urania systems with lattice-statics and MD approach, the overall interactions are defined by the sum of long-range and short-range contributions. The long-range interactions for all the potentials are described by the Coulombic interaction.

$$V_{Coul}(r_{ij}) = \frac{1}{2}\sum_{i=1}^{N}\left\{\sum_{j\neq i}\frac{q_i q_j}{r_{ij}}\right\} \tag{2}$$

where N is the total number of ions in the system, q_i, q_j are the magnitude of charges on ions i and j, and r_{ij} is the separation between ions i and j. The Ewald sum approach is used to estimate the Columbic interactions within a finite cut-off distance.

The short-range interactions are described predominantly by strong repulsive interactions. All the potentials considered in this article describes the short-range interaction by the Buckingham potential [23] form, which is given as:

$$V_{Buck}(r_{ij}) = A_{ij}\exp(-r_{ij}/\rho_{ij}) - C_{ij}/r_{ij}^6 \tag{3}$$

where r_{ij} is the separation between two ions i and j; and A, ρ, and C are free parameters. Pot5 and Pot6 includes an additional Morse potential [24], which is used to describe the covalent bonding in the system. The Morse potential is given as:

$$V_{Morse}(r_{ij}) = D_{ij}\left\{\left[1-\exp\left(-\beta_{ij}\left(r_{ij}-r_{ij}^*\right)\right)\right]^2 - 1\right\} \tag{4}$$

where r_{ij} is the separation between two ions i and j; and D, β and r_{ij}^* are free parameters. All the potential parameters are given in Tables 2a and 2b.

The General Utility Lattice Program (GULP) [25,26] was used to predict the structural and elastic properties discussed in this article. The simulations were performed within a 30% substitution of the U^{4+} ions, which is in line with the concentration ranges reported in the literature for UO_2 systems. In the input structures, the substituted ions were randomly distributed in the urania matrix for all the concentrations. Following the work by Xu et al. [27] on similar Fluorite system, a $4\times4\times4$ supercell (768 atoms for bulk phases) was used to perform all the calculations.

Table 1
List of atomic interactions available for Actinides and Lanthanides produced during UO_2 fuel cycle with specific charge.

Referred as	Grimes01 Pot1 [15]	Grimes02 Pot2 [16]		Grimes03 Pot3 [17]		Nadeem Pot4 [18]	Osaka Pot5 [19]	Uchida Pot6 [20,21]	
Actinides									
Th						4+	4+	4+	
U	4+	4+		4+	3+	4+	4+	4+	
Np							4+		
Pu		4+		4+	3+		4+		
Am							4+	4+	3+
Cm									
Lanthanides									
Ce	4+	4+	3+			4+			
Nd				3+					
Pm									
Sm		3+		3+					
Eu				3+					
Gd		3+		3+			3+		

Table 2a
Interatomic potential parameters for core-shell models (Pot1, Pot2, Pot3, and Pot4) used to simulate various Lanthanides and Actinides substitution in urania. All the potentials listed here are formal charge models.

Species	Buckingham parameters			Core-shell parameters			Ref.
	A (eV)	ρ (Å)	C (eV Å^6)	q_{core} [e]	q_{shell} (e)	k_2 (eV Å^{-2})	
							Pot1[15]
O^{2-}–O^{2-}	108.00	0.3800	56.06	2.40	−4.40	296.80	
U^{4+}–O^{2-}	2494.20	0.34123	40.16	−2.54	6.54	98.24	
U^{4+}–U^{4+}	18600.00	0.27468	32.64				
Ce^{4+}–O^{2-}	1984.20	0.34940	26.44	11.30	−7.30	1957.00	
Ce^{4+}–U^{4+}	101860.00	0.24076	23.87				
							Pot2[16]
O^{2-}–O^{2-}	9547.96	0.2192	32.0	0.04	−2.04	6.30	
U^{4+}–O^{2-}	1761.775	0.35642	0.0	4.10	−0.10	160.00	
Pu^{4+}–O^{2-}	1682.08	0.3542	0.0	4.00			
Ce^{4+}–O^{2-}	1809.68	0.3547	20.40	4.20	−0.20	177.84	
Ce^{3+}–O^{2-}	2010.18	0.3449	23.11	3.00			
Sm^{3+}–O^{2-}	1944.44	0.3414	21.49	3.00			
Gd^{3+}– O^{2-}	1885.75	0.3399	20.34	3.00			
							Pot3[17]
O^{2-}–O^{2-}	9547.96	0.2192	32.0	0.04	−2.04	32.00	
U^{4+}–O^{2-}	1761.775	0.356421	0.0	4.00			
Pu^{4+}–O^{2-}	1762.84	0.35420	11.48	4.00			
U^{3+}–O^{2-}	1165.65	0.376582	0.0	3.00			
Pu^{3+}–O^{2-}	1150.745	0.37430	12.10	3.00			
Nd^{3+}–O^{2-}	1995.20	0.34300	22.59	3.00			
Sm^{3+}–O^{2-}	1944.44	0.34140	21.49	3.00			
Eu^{3+}–O^{2-}	1925.71	0.34030	20.59	3.00			
Gd^{3+}– O^{2-}	1885.75	0.3399	20.34	3.00			
							Pot4[18]
O^{2-}–O^{2-}	25.41	0.6937	32.32	0.513	−2.513	20.53	
U^{4+}–O^{2-}	9296.65	0.2796	90.00	5.00	−1.00	134.00	
Th^{4+}–O^{2-}	8638.50	0.2856	70.00	4.64	−0.64	110.00	
Ce^{4+}–O^{2-}	7549.87	0.2831	70.00	2.75	1.25	222.00	

The random distribution of substituted ions depends on the configurational space available in the input structure and thus on the size of the simulation supercell. There are different approximations that can be employed to establish solid solution configuration using smaller supercells. These methods are extremely attractive for first-principles calculation, which is limited by system size. The approximations are (i) coherent potential approximation (CPA), (ii) cluster expansion (CE), and (iii) special-quasirandom structure (SQS) [28]. While CPA and CE are useful for first-principles calculation, SQS method can be used for both first-principles and atomistic simulations. In the SQS method, structures are generated which mimics the correlation functions of an infinite random system within a finite supercell. For a random alloying of Al–Ti system, von Pezold et al. [28] reported that the SQS method with a $2 \times 2 \times 2$ (32 atom) supercell resulted in similar elastic properties as a randomly distributed alloy system with $4 \times 4 \times 4$ supercell containing 256 atoms. Since, all the calculations in this manuscript are performed with a $4 \times 4 \times 4$ supercell containing 768 atoms, the random distribution of substituted ions are used to evaluate the structural and elastic properties.

For all the substituted ions, the relationship between the Shannon ionic radii [29] and the atomic number is presented in Fig. 1. Fig. 1a illustrates the ionic radii variation with atomic number for Lanthanides, while Fig. 1b illustrates the variation for Actinides. In general, the ionic radii of 3+ ions are larger than 4+ ions, which is as expected. The ionic radius decreases with the increase in atomic number for a particular charge state. The ionic radii of 3+ ions are presented with two different coordination numbers (CN = 6 and 8). Since we are substituting 3+ ions in UO_2-matrix, we have considered the ionic radii with CN = 8 for discussion.

There are different mechanisms associated with 4+ and 3+ ion substitution. Substitution of 4+ ions at the cation sites of the urania

matrix ($U_{1-x}A_xO_2$) does not change the electrostatic of the system. Therefore, the change in lattice parameter due to 4+ ion substitution can be assigned to the change in the radii of the substituted ions, i.e. the elastic effect. A smaller ionic radius relative to U^{4+} ion will create local compression, thereby is expected to reduce the lattice parameter. Similarly, a larger ionic radius will create local tension, which will tend to increase the lattice parameter. On the other hand, we have to consider both elastic and electrostatic effects to understand the response of 3+ ions substitution in the urania matrix ($U_{1-2x}A_{2x}O_{2-x}$). Xu et al. [27] have reported the possible effects of 3+ ions in a CeO_2 matrix. Similar structural response is expected for 3+ ion substitution in UO_2. The electrostatic response for 3+ ion substitution should increase the lattice parameter due to (i) the reduction in electrostatic attraction and (ii) increase in electrostatic repulsion due to the oxygen vacancies. The elastic response due to the substitution of a larger ionic radius ion (3+ ions have larger ionic radii than U^{4+} ion, see Fig. 1) will increase the lattice parameter. However, the increase in the number of vacancies due to the increase in the 3+ ions in the system reduces the density of the overall system. In order to increase the density of the system, this effect will try to reduce the lattice parameter. Hence, there are three factors acting towards increasing the lattice parameter, and one towards reducing the lattice parameter. The overall effect for different 4+ and 3+ ions are discussed in detail.

3. Results

3.1. Pristine UO_2

Each interatomic potential that we employ has been fit to pristine UO_2 properties. The bulk properties of UO_2 predicted from each potential are summarized in Table 3. These include the lattice parameter, elastic properties, dielectric constants and phonon properties. As seen from the table, most pristine, pure UO_2 properties are well predicted by these interatomic potentials. A detailed review is provided by Govers et al. [30,31]. Except Pot4, all other potentials underestimated the lattice parameter. Pot1 underestimates the lattice parameter by ~0.15%, while Pot6 by ~0.45% compared to <0.1% by the rest of the potentials. Pot4 overestimates the lattice parameter by ~0.1%. Most of the potentials overestimated individual elastic constants. Pot5 predicts the C_{11} value within 10% of the experimental value, but it severely underestimates (~50%) the C_{12} value. All the potentials predict positive phonon frequencies, indicating the Fluorite structure to be stable.

We have calculated the anisotropy of the UO_2 lattice as well as polycrystalline elastic moduli, which are not calculated before. The individual elastic constants are used to calculate the Zener anisotropy factor (Z) and the properties of polycrystalline UO_2. The Z factor describes the anisotropy in the cubic system. Using C_{11}, C_{12}, and C_{44}, the only non-zero tensor quantities for a cubic system, Z can be defined as:

$$Z = \frac{2C_{44}}{C_{11} - C_{12}} \tag{5}$$

where $Z = 1$ indicates a perfectly isotropic system, and $Z < 1$ indicates an anisotropic system. The Z value calculated from experimental elastic constants is 0.44 (data in Table 3) and 0.47 (reported by Belle and Berman [32]). Thus, $Z < 1$ indicates that the UO_2 system is anisotropic and the elastic moduli values will be a maximum along the [1 0 0] or cube direction and a minimum along the [1 1 1] or octahedral direction. Therefore, the value of the elastic properties along the octahedral direction is expected to be 44% of the axial direction. The estimated Young's modulus along the [1 1 1] direction is reported in Table 3. Belle and Berman [32] reported the experimentally measured Young's modulus along [1 1 1] direction and it is ~52% of the axial directions. This value is slightly higher than the Z value calculated using experimental elastic constants. Table 3 shows the anisotropy factor values calculated for each UO_2 potential using Eq. (5), which is estimated to be 0.47 for Pot1, 0.59 for Pot2 and Pot3, 0.66 for Pot4, and 0.69 for Pot6. The Z value for Pot5 is estimated to be 0.30 mainly due to the severe underestimation of C_{12}.

Table 2b
Interatomic potential parameters for rigid ion models (Pot5 and Pot6) used to simulate various Lanthanides and Actinides substitution in urania. All the potentials listed here are partial charge models.

Species	Buckingham parameters			Morse parameters			Ref.
	A (eV)	ρ (Å)	C (eV Å^6)	D (eV)	β_{ij} (1/Å)	r^*_{ij} (Å)	
							Pot5[19]
$O^{1.2-}$–$O^{1.2-}$	2346.1488	0.32	4.14616				
$U^{2.4+}$–$U^{2.4+}$	442.2081	0.32	0.0				
$U^{2.4+}$–$O^{1.2-}$	1018.5705	0.32	0.0	0.78101	1.25	2.369	
$Th^{2.4+}$–$Th^{2.4+}$	17.0261	0.82	0.0				
$Th^{2.4+}$–$O^{1.2-}$	61.4295	0.57	0.0	1.21500	1.90	2.360	
$Np^{2.4+}$–$Np^{2.4+}$	20027.9343	0.16	0.0				
$Np^{2.4+}$–$O^{1.2-}$	4530.9265	0.24	0.0	0.45559	3.27	2.339	
$Pu^{2.4+}$–$Pu^{2.4+}$	32610.2942	0.16	0.0				
$Pu^{2.4+}$–$O^{1.2-}$	5330.4009	0.24	0.0	0.56406	1.56	2.339	
$Am^{2.4+}$–$Am^{2.4+}$	3568.4382	0.16	0.0				
$Am^{2.4+}$–$O^{1.2-}$	2549.5744	0.24	0.0	0.37315	3.98	2.339	
$Gd^{1.8+}$–$Gd^{1.8+}$	139021.40	0.16	0.0				
$Gd^{1.8+}$–$O^{1.2-}$	8643.0870	0.24	0.0	1.27132	0.80	2.353	
							Pot6[20,21]
$O^{1.35-}$–$O^{1.35-}$	919.17	0.332	17.36				
$U^{2.7+}$–$U^{2.7+}$	$2.48 \times 10^{+13}$	0.072	0.0				
$U^{2.7+}$–$O^{1.35-}$	55918.39	0.202	0.0				
$Th^{2.7+}$–$O^{1.35-}$	31321.23	0.220	0.0				
$Am^{2.7+}$–$Am^{2.7+}$	$2.73 \times 10^{+12}$	0.075	0.0				
$Am^{2.7+}$–$O^{1.35-}$	42635.38877	0.203	0.0				
$Am^{2.025+}$–$Am^{2.025+}$	$5.69 \times 10^{+15}$	0.060	0.0				
$Am^{2.025+}$–$O^{1.35-}$	68417.58793	0.196	0.0				

Note that due to the partial charge definitions for Pot5 all the +4 charges are defined as an effective charge of +2.4 e and the +3 charges are assigned +1.8 e; while for Pot6 the corresponding charges are +2.7 e and +2.025 e respectively.

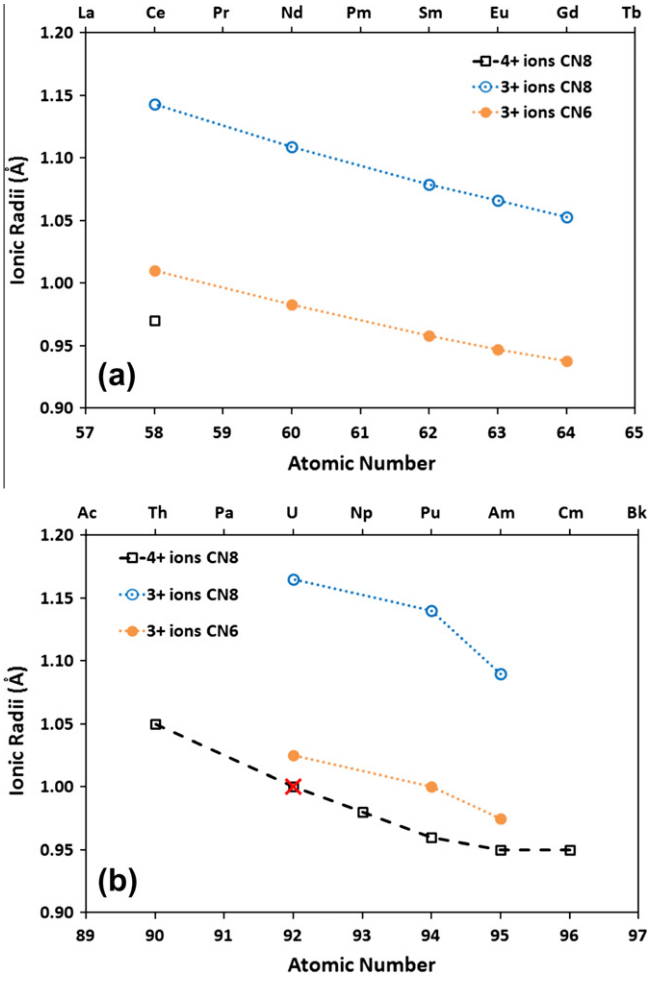

Fig. 1. Shannon ionic radii of 4+ ions with eight coordination number and 3+ ions with eight and six coordination numbers for (a) Lanthanides and (b) Actinides. The data with the red cross in (b) represents the ionic radius of U^{4+} ion (1.0 nm).

Using the individual elastic constants, and the Viogt-Reuss-Hill (VRH) approximation, we calculated the polycrystalline elastic moduli. The VRH approximation gives a lower (G_R) and upper bound (G_v) for the shear modulus, and is given as [27,33]:

$$G_R = \frac{5(C_{11}-C_{12})\times C_{44}}{4C_{44}+3(C_{11}-C_{12})} < G < G_v = \frac{C_{11}-C_{12}+3C_{44}}{5} \tag{6}$$

Since the bulk modulus for the single and polycrystalline samples are exactly the same, the bulk and shear moduli values can be used to estimate the Young's modulus of polycrystalline UO_2, which is given as:

$$E_R = \frac{9B\times G}{(3B+G)}, \quad \text{where } G = G_R \text{ or } G_v \tag{7}$$

Table 3 lists the lower and upper bounds of shear and Young's modulus calculated from experiment and empirical potentials.

After analyzing the structural and elastic properties of pure UO_2, we are interested in characterizing the variation of these properties due to the substitution of heavy ions. Since the lattice parameter changes due to substitution of 4+ and 3+ ions at a constant temperature, we have estimated the lattice parameter variation with a physical parameter defined as chemical expansion.

3.2. Chemical expansion

Chemical substitution changes the lattice parameter and its effect can be analyzed by defining a chemical expansion, which is analogous to thermal expansion. While thermal expansion measures the variation in lattice parameter with change in temperature at constant pressure, chemical expansion measures the change in lattice parameter due to a change in chemical formula at constant temperature. Therefore, chemical expansion depends on the type of ions substituted in the host matrix (in this article it is urania matrix). While thermal expansion for most of the materials is positive with increase in temperature, the chemical expansion may be either positive or negative depending on the substituted ions (ion type, ionic radii, charge). Thus, we define the chemical expansion in UO_2 as the change in lattice parameter due to substitution with respect to the lattice parameter of pure UO_2. The chemical expansion is defined as [34]:

$$\varepsilon_C = \left.\frac{(a-a_0)}{a_0}\right|_{T=\text{Constant}} \tag{8}$$

where a is the lattice parameter measured at any concentration, and a_0 is the lattice parameter of UO_2 perfect lattice. The measurements are performed at a constant temperature. The chemical expansion coefficient [34] is generally defined as

Table 3
Comparison of bulk properties of UO_2 calculated from different interatomic potentials with experiment.

	Experiment	Pot1	Pot2	Pot3	Pot4	Pot5	Pot6
Lattice parameter (Å)	5.4698	5.4615	5.4681	5.4682	5.4749	5.4654	5.4449
Lattice energy (eV/UO_2)	−106.700	−105.6762	−104.502	−104.501	−107.479	−45.589	−51.005
C_{11} (GPa)	389	524	532	532	626	419	434
C_{12} (GPa)	119	147	122	122	187	59	120
C_{44} (GPa)	60	89	121	122	144	55	109
Poisson's ration		0.219	0.187	0.187	0.230	0.124	0.217
Compressibility (10^{-3}/GPa)		3.66	3.86	3.86	3.00	5.58	4.45
Static dielec. const.	24.0	13.1	18.1	7.8	19.1	3.8	3.2
High. freq. di const.	5.3	5.3	5.7	2.0	4.9		
Phonons at Γ (293 K)							
T mode (cm^{-1})	280.0	344.0	178.9	294.9	238.4	295.0	379.5
L mode (cm^{-1})	450.0	533.3	282.2	444.6	427.6	577.2	570.7
Anisotropy factor (Z)[a]	0.44	0.47	0.59	0.59	0.66	0.30	0.69
$B_{single\_crystal}$ (GPa)	204	273	259	259	333	179	225
$G_{single\_crystal}$ (GPa)		113	150	150	171	90	126
$Y_{single\_crystal}$ [100] (GPa)	385	459	486	486	540	405	382
$Y_{single\_crystal}$ [111] (GPa)[b]	170	218	287	289	354	123	265
$B_{polycrystal}$ (GPa)	204	273	259	259	333	179	225
$G_{polycrystal}$ (GPa)	77–90	113–129	145–155	145–155	167–174	76–105	124–128
$Y_{polycrystal}$ [100] (GPa)	205–235	298–334	366–387	367–387	429–445	199–263	314–323

[a] Belle and Berman [32] reported the value of $Z = 0.47$ for UO_2.
[b] Young's modulus along [111] direction is calculated using Z values.

$$\alpha_C = \frac{\varepsilon_C}{\Delta\delta} \tag{9}$$

where $\Delta\delta$ is change in the oxygen-vacancy concentration in the system, and δ is the measure of the oxygen-vacancy concentration.

However, since we are focusing on both 4+ and 3+ ion substitution in UO_2, and the oxygen-vacancy concentration is kept fixed for a particular stoichiometry with atomic precision, the use of $\Delta\delta$ for chemical expansion coefficient is not very useful. Therefore, we have used the chemical expansion (ε_c) variation with respect to the ionic radius of the substituted ion. Thus, Eq. (9) is modified as

$$\alpha_C = \frac{\varepsilon_c}{\Delta r} \tag{10}$$

where Δr is change in the ionic radius of the substituted ion with respect to U^{4+} ion. For example, comparing the ionic radii of Ce^{4+} (0.97 Å) and U^{4+} (1.00 Å), the value of $\Delta r = -0.03$ Å. Again Eq. (8) can be compared with the coefficient of linear thermal expansion as

$$\begin{aligned} \frac{(a-a_0)}{a_0} &= \alpha_T \Delta T \\ \frac{(a-a_0)}{a_0} &= \alpha_C \Delta r \end{aligned} \tag{11}$$

where α_T is coefficient of linear thermal expansion, ΔT is the change in temperature and α_C is chemical expansion coefficient. Since, all the simulations are performed with single crystalline urania system, the variation in change in length is equivalent to measuring the change in lattice parameter

$$\frac{(a-a_0)}{a_0} = \frac{(L-L_0)}{L_0} \tag{12}$$

where L is the length of the supercell measured with substituted ions, and L_0 is the length of the supercell for perfect UO_2. In addition to the above analysis, the ε_c values can be used to get an indication of the equivalent change in temperature (ΔT_{eq}) necessary to achieve the same amount of lattice parameter variation in pure UO_2. This is calculated by considering the ε_c values and the coefficient of thermal expansion reported for bulk UO_2 $11.8 \times 10^{-6}\,K^{-1}$ [35] from experiment, and using

$$\varepsilon_C = \alpha_{T,bulkUO_2} \Delta T_{eq} \tag{13}$$

3.3. Ce^{4+} substitution in UO_2

Before discussing the results on the effect of Lanthanide and Actinide substitution in UO_2, we have analyzed the atomistic model for Ce^{4+} substitution since experimental characterization of lattice parameter is available for $U_{1-x}Ce_xO_2$ system [10]. Thus we used Pot1, Pot2 and Pot4 potentials to evaluate the change in lattice parameter for $U_{1-x}Ce_xO_2$ system, where $x < 0.3$. It is important to note that Pot1, Pot2 and Pot4 are the only potentials which describe the Ce^{4+} ion interaction in UO_2.

Fig. 2 illustrates the comparison of the relative change in lattice parameter with fraction of Ce. The relative change in lattice parameter is calculated with respect to the bulk UO_2 lattice parameter predicted at $x = 0$. Following the results presented in Table 3, the lattice parameters predicted for pure UO_2 are 5.4615 Å, 5.4681 Å, and 5.4749 Å for Pot1, Pot2, and Pot4 respectively. Comparing these lattice parameters, Pot2 quantitatively compares well with experiment (5.4698 Å [10]), while Pot1 underestimates and Pot4 overestimates the bulk UO_2 lattice parameter. Therefore, a relative change in lattice parameter is more meaningful for comparison with experimental values of Ce^{4+} substitution.

Fig. 2 clearly shows that all the potentials predicted the variation in lattice parameter of $U_{1-x}Ce_xO_2$ system similar to experiment. Pot1 shows a larger deviation at larger concentration of Ce^{4+} in the urania matrix. Using the atomistic models we have successfully calculated the variation in structural property of a Ce^{4+} ion substituted urania system. Overall, the results show that substitution of a smaller ionic radius cation (Ce^{4+} = 0.97 Å compared to U^{4+} = 1.00 Å) reduces the overall lattice parameter of the system.

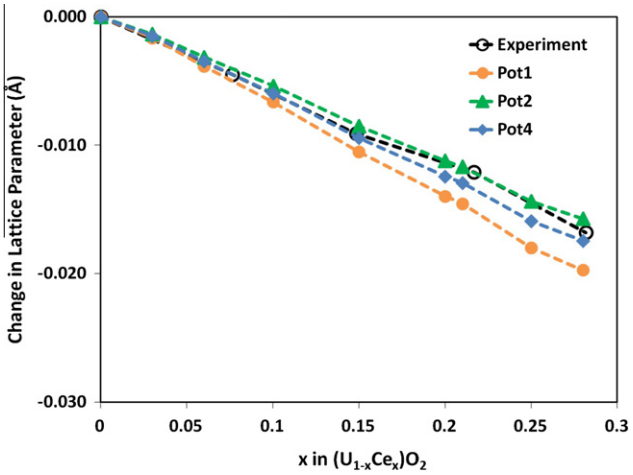

Fig. 2. Relative variation in lattice parameter due to 4+ ion substitution in $U_{1-x}Ce_xO_2$ system with respect to the bulk UO_2 lattice parameter.

These lattice variations predicted for the $U_{1-x}Ce_xO_2$ system can be used to estimate the chemical expansion, expansion coefficient, change in lattice parameter and equivalent temperatures. Table 4 lists the comparison of chemical expansion and chemical expansion coefficients for $U_{1-x}Ce_xO_2$ system. The predicted ε_c and α_C values with all the three empirical potentials are comparable to the experimental values for $U_{1-x}Ce_xO_2$ system with $x < 0.30$. The results show that the lattice contraction observed for $U_{0.72}Ce_{0.28}O_2$ system, is equivalent to reducing the temperature by ~273 ± 31 K for bulk UO_2. Similar analysis on Th^{4+} ions are recently published by Behera and Deo [36].

3.4. Substitution of other 4+ ions

Now we have considered the substitution of other 4+ Lanthanides and Actinides in urania ($U_{1-x}A_xO_2$). The composition considered for substitution is ~20% or $U_{1-x}A_xO_2$, where $x = 0.2$ and A = Am, Pu, Ce, Np, and Th. Fig. 3 illustrates the variation in lattice parameter with ionic radii of the substituted A ions in the UO_2 matrix. As ionic radius of the substituted ion increases, the lattice parameter increases. In Fig. 3, we present the data with respect to the ionic radius of U^{4+}. Thus, the substitution of a lower ionic radius ion relative to U^{4+} ion decreases the overall lattice parameter, while a relatively larger ionic radius ion increases the average lattice parameter. This is in line with the discussion in Section 2, and the overall variation in lattice parameter is assigned to the elastic effect for 4+ ion substitution.

3.5. Substitution of 3+ ions

For a fixed charge model, such as the one considered for this study, the substitution of 3+ ions in the UO_2 system requires the generation of oxygen vacancies in order to achieve a charge neutral system. Due to the change in charge of the substituted ion and the ionic radius, both elastic and electrostatic effects are present in $U_{1-2x}A_{2x}O_{2-x}$ system. Here "A" may be the Lanthanides and Actinides substituted in the UO_2 matrix or may by U^{3+}, which has a significantly higher radius than U^{4+}. First the effect of U^{3+} ion substitution is discussed followed by the effect of other 3+ Lanthanides and Actinides.

Table 4
Chemical expansion coefficients calculated for Ce^{4+} ion substitution in $U_{1-x}Ce_xO_2$ system using Pot1, Pot2 and Pot4 potentials compared to experiment [10]. The symbols: x is the concentration of substituted ion, a_0 is the lattice parameter of UO_2 perfect lattice, a is the lattice parameter measured at a particular concentration, Δa is change in the lattice parameter, ε_C is change chemical expansion, Δr is change in the ionic radius, α_C is the chemical expansion coefficient, and ΔT_{eq} is the equivalent temperature.

x	a_0 (Å)	a (Å)	Δa (Å)	ε_C	Δr (Å)	α_C ($Å^{-1}$)	ΔT_{eq} (K) [a]
Experiment							
0	5.4698						
0.0763		5.4653	−0.0045	−0.0008	−0.03	0.027	−70
0.1484		5.4607	−0.0091	−0.0017	−0.03	0.055	−141
0.2168		5.4577	−0.0121	−0.0022	−0.03	0.074	−187
0.2817		5.4530	−0.0168	−0.0031	−0.03	0.102	−260
Pot1							
0	5.4615						
0.06		5.4577	−0.0039	−0.0007	−0.03	0.024	−60
0.15		5.4510	−0.0105	−0.0019	−0.03	0.064	−163
0.21		5.4470	−0.0145	−0.0027	−0.03	0.089	−226
0.28		5.4418	−0.0197	−0.0036	−0.03	0.120	−306
Pot2							
0	5.4681						
0.06		5.4650	−0.0031	−0.0006	−0.03	0.019	−49
0.15		5.4596	−0.0085	−0.0016	−0.03	0.052	−132
0.21		5.4565	−0.0117	−0.0021	−0.03	0.071	−181
0.28		5.4524	−0.0157	−0.0029	−0.03	0.096	−244
Pot4							
0	5.4749						
0.06		5.4714	−0.0035	−0.0006	−0.03	0.021	−54
0.15		5.4655	−0.0094	−0.0017	−0.03	0.057	−146
0.21		5.4620	−0.0129	−0.0024	−0.03	0.079	−200
0.28		5.4575	−0.0174	−0.0032	−0.03	0.106	−270

[a] The value of ΔT_{eq} is calculated based on experimental thermal expansion coefficient of UO_2 ($\alpha_T = 11.8 \times 10^{-6}\,K^{-1}$ by Fink [35]).

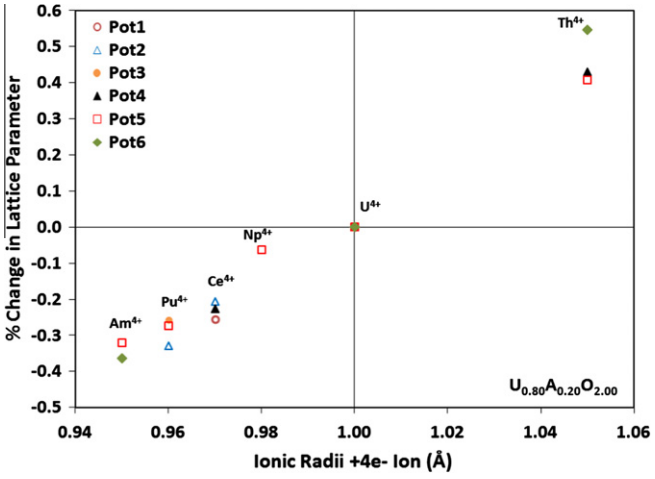

Fig. 3. Variation in lattice parameter due to 4+ ion substitution in $U_{1-x}A_xO_2$ system, where $x = 0.20$.

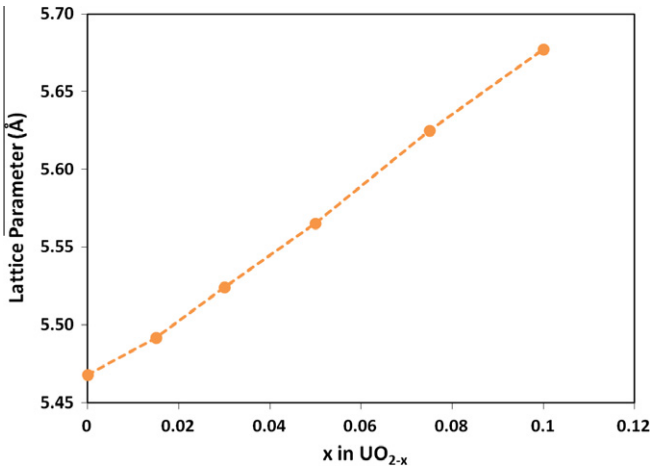

Fig. 4. Variation in lattice parameter due to U^{3+} ion substitution in UO_{2-x} system using Pot3. Pot3 is the only potential which can describe U^{3+} ion substitution.

3.5.1. U^{3+} ion substitution

The overall effect of U^{3+} ion substitution on the lattice parameter is illustrated in Fig. 4. This figure plots the variation of lattice parameter with substitution of U^{3+} in $U_{1-2x}A_{2x}O_{2-x}$ giving, in this special case, UO_{2-x}. The maximum value of substitution characterized is $x = 0.1$, which corresponds to replacement of 20% of the original UO_2 matrix by U^{3+} and vacancies. The predicted variation of lattice parameter for UO_{2-x} system shows an overall increase in the lattice parameter with increase in x. This increase can be explained due to the larger ionic radii of the U^{3+} ion, and the reduced electrostatic attraction.

Fig. 5 shows the variation in elastic constants for <20% U^{3+} substitution in urania. Due to the increase in the lattice parameter, it is expected that the UO_{2-x} will be mechanically softer than UO_2, which is evident from the moduli predictions for the UO_{2-x} system. The bulk, shear, and Young's modulus decreases by ~29%, 38%, and 43% for ~20% U^{3+} substitution or $UO_{1.90}$ system.

3.5.2. Lanthanide 3+ and Actinide 3+ ion substitution

Here the elastic and electrostatic effect of 3+ Lanthanide and Actinide substitution is studied for ~20% substitution ($U_{0.80}A_{0.20}O_{1.90}$), which corresponds to $x = 0.1$ and allows for direct comparison with the 4+ ion substitution corresponding to $U_{0.80}A_{0.20}O_{2.00}$. Fig. 6 illustrates the change in lattice parameter with ionic radii of the substituted ions for $U_{0.80}A_{0.20}O_{1.90}$. The results show that lattice parameter increases with the increase in ionic radius of the substituted 3+ ion. The change in lattice parameter in Fig. 6 can be directly compared with 4+ ion substitution. The rate of increase in the lattice parameter for 3+ ions is relatively less than the 4+ ions. However, in Fig. 6, Nd^{3+}, Pu^{3+}, Ce^{3+} and

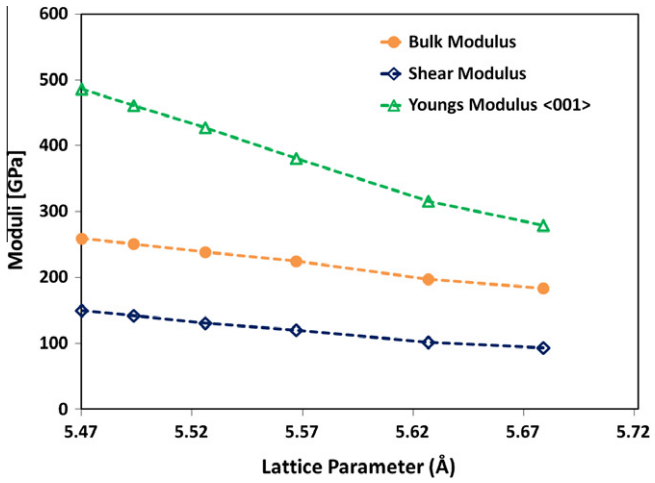

Fig. 5. Variation in bulk, shear, and Young's modulus in UO_{2-x} system using Pot3.

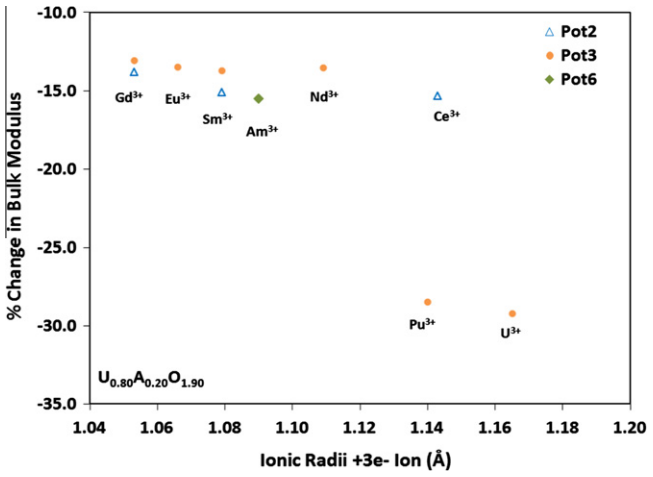

Fig. 7. Variation in bulk modulus due to 3+ ion substitution in $U_{1-2x}A_{2x}O_{2-x}$ system, where $2x = 0.20$.

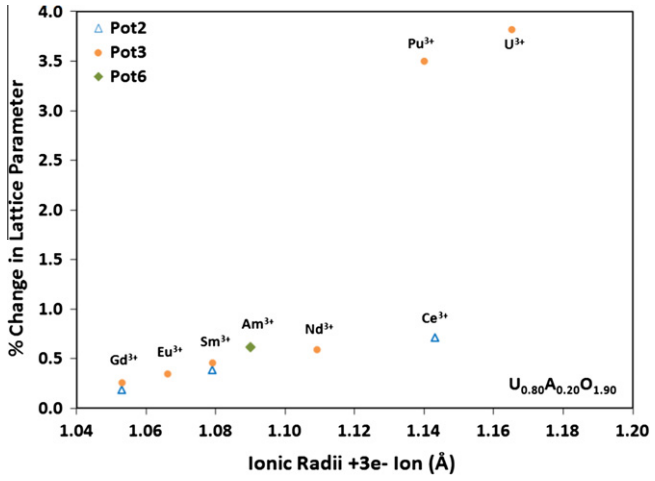

Fig. 6. Variation in lattice parameter due to 3+ ion substitution in $U_{1-2x}A_{2x}O_{2-x}$ system, where $2x = 0.20$.

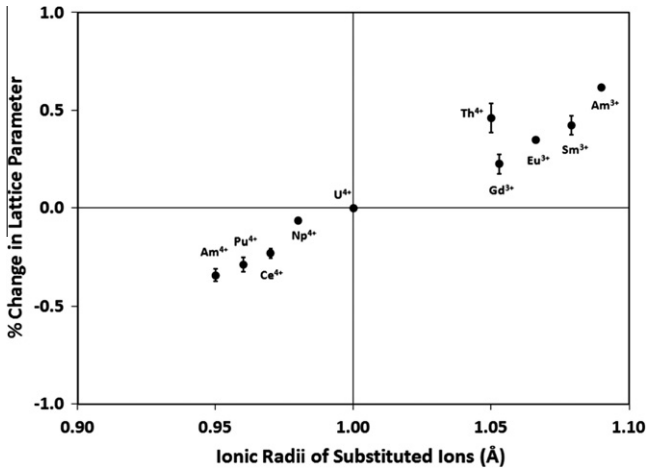

Fig. 8. Effect of 4+ and 3+ ion substitutions in uranium dioxide, where the stoichiometric fraction of A is 0.20. The error bars are the error associated with the predicted lattice parameter variation for a particular substituted ion with different potentials.

U^{3+} ions do not follow the lattice parameter variation trend. These ions show a larger change in ionic radius (>10%) compared to the host U^{4+} (U^{4+} = 1.00 Å, Nd^{3+} = 1.109 Å, Pu^{3+} = 1.14 Å, Ce^{3+} = 1.143 Å, and U^{3+} = 1.165 Å). These larger ions lead to a greater strain in the lattice, which causes the observed deviation in the overall lattice parameter. Therefore, these elements are not considered for further discussion. Fig. 7 shows the variation in bulk modulus as a function of ionic radii, which shows ~13–16% reduction in the bulk modulus values. The shear and Young's moduli values show similar reduction of 17–23% and 19–24% respectively. Therefore, 3+ ion substitution reduces the mechanical properties of urania matrix.

4. Discussions and conclusions

The effect of 4+ and 3+ ion substitutions are combined to analyze the overall effect on lattice parameter of the urania matrix. This is achieved by plotting the 20% cation substitution in the urania matrix for both 4+ and 3+ ions. In effect this combines the results shown in Figs. 3 and 6. Fig. 8 illustrates that most of the Lanthanide and Actinide 4+ ions (except Th^{4+}) decreases the overall lattice parameter, which is guided by the smaller size of the substituted 4+ ions compared to U^{4+}. However, all the 3+ ions increase the lattice parameter of the urania matrix. The error bars shown in Fig. 8 are the error associated with the predicted lattice parameter variation with different potentials. The error bars shown in other plots in the manuscript are also the variation in properties by different interatomic potentials. Using Eq. (8), the average chemical expansion is estimated for all the Lanthanides and Actinides considered in this study. Fig. 9a plots the change in chemical expansion with the ionic radii of the substituted ions, which shows a linear trend in chemical expansion with ionic radius. Even though the slopes are similar, 4+ and 3+ ions do not follow the same line (between Th^{4+} = 1.05 Å, and Gd^{3+} = 1.053 Å). This deviation can be attributed to the additional electrostatic effect and oxygen vacancies associated with the 3+ ions substitution.

The chemical expansion coefficient is estimated by Eq. (10) and is presented in Fig. 9b as a function of ionic radius. This plot shows that most of the 4+ ions have a larger chemical expansion coefficient than the 3+ ions. The chemical expansions observed for 20% substitution have been used to estimate the equivalent temperatures in pure UO_2 (Fig. 10, Tables 5 and 6). For example, considering the effect of 20% Am substitution, the reduction in chemical expansion for Am^{4+} is equivalent to decreasing the temperature by ~290 K in pure UO_2. Similarly the increase in chemical expan-

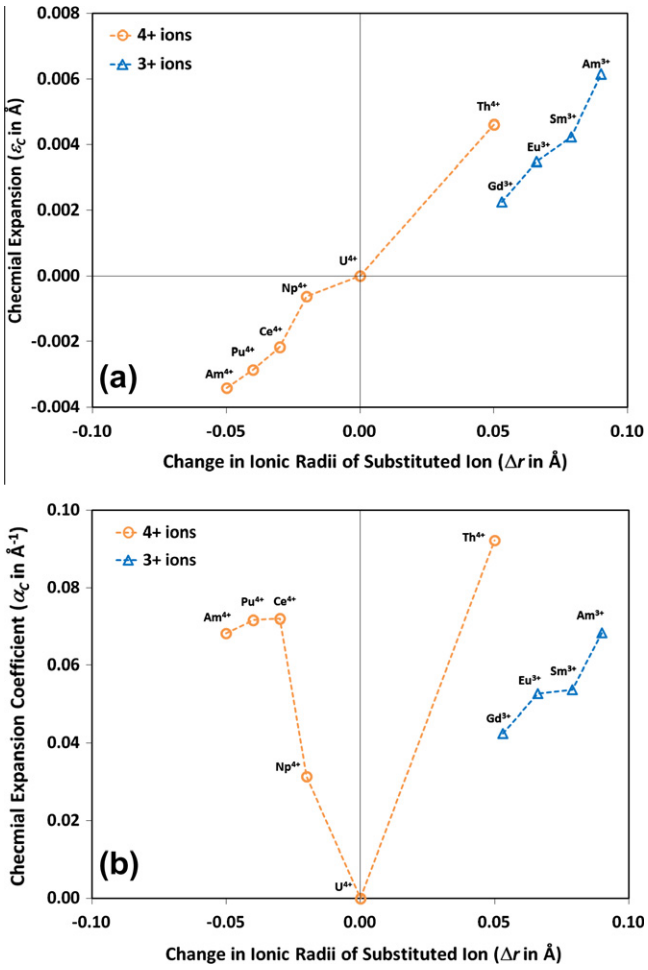

Fig. 9. Comparison of (a) chemical expansion (ε_C) and (b) chemical expansion coefficient (α_C) of 4+ and 3+ ion substitution in $U_{0.80}A_{0.20}$ system. The (ε_C) increases with an increase in the substituted ionic radii with respect to U^{4+} ionic radius, and vice versa. The (α_C) is always positive and increases with the increase in the magnitude of the change in ionic radii.

Table 5
Chemical expansion coefficients calculated for +4 ion substitution in $U_{0.80}A_{0.20}O_2$ system ($x = 0.20$) using empirical potentials (for the meaning of the symbols please refer Table 4).

Potential	a_0 (Å)	A ion	Δr (Å)	a (Å)	ε_C	α_C (Å^{-1})	ΔT_{eq} (K)[a]
Pot1	5.4681	Ce^{4+}	−0.03	5.4476	−0.0026	0.085	−217
Pot2	5.4681	Pu^{4+}	−0.04	5.4502	−0.0033	0.082	−279
		Ce^{4+}	−0.03	5.4569	−0.0021	0.068	−174
Pot3	5.4682	Pu^{4+}	−0.04	5.4541	−0.0026	0.064	−218
Pot4	5.4749	Ce^{4+}	−0.03	5.4625	−0.0023	0.076	−192
		Th^{4+}	+0.05	5.4984	+0.0043	0.086	+364
Pot5	5.4654	Am^{4+}	−0.05	5.4479	−0.0032	0.064	−271
		Pu^{4+}	−0.04	5.4505	−0.0027	0.068	−231
		Np^{4+}	−0.02	5.4620	−0.0006	0.031	−53
		Th^{4+}	+0.05	5.4877	+0.0041	0.082	+345
Pot6	5.4449	Am^{4+}	−0.05	5.4252	−0.0036	0.073	−307
		Th^{4+}	+0.05	5.4747	+0.0055	0.109	+463

[a] The value of ΔT_{eq} is calculated based on experimental thermal expansion coefficient of UO_2 ($\alpha_T = 11.8 \times 10^{-6}\ K^{-1}$ by Fink [35]).

Table 6
Chemical expansion coefficients calculated for +3 ion substitution in $U_{0.80}A_{0.20}O_{1.90}$ system ($x = 0.20$) using empirical potentials (for the meaning of the symbols please refer Table 4).

Potential	a_0 (Å)	A ion	Δr (Å)	a (Å)	ε_C	α_C (Å^{-1})	ΔT_{eq} (K)[a]
Pot2	5.4681	Gd^{3+}	0.053	5.4784	+0.0019	0.036	+159
		Sm^{3+}	0.079	5.4894	+0.0039	0.049	+330
		Ce^{3+}	0.143	5.5073	+0.0072	0.050	+607
Pot3	5.4682	Gd^{3+}	0.053	5.4824	+0.0026	0.049	+221
		Eu^{3+}	0.066	5.4872	+0.0035	0.053	+295
		Sm^{3+}	0.079	5.4932	+0.0046	0.058	+389
		Nd^{3+}	0.109	5.5007	+0.0060	0.055	+504
		Pu^{3+}	0.140	5.6599	+0.0351	0.250	+2971
		U^{3+}	0.165	5.6771	+0.0382	0.232	+3238
Pot6	5.4449	Am^{3+}	0.090	5.4785	+0.0062	0.068	+522

[a] The value of ΔT_{eq} is calculated based on experimental thermal expansion coefficient of UO_2 ($\alpha_T = 11.8 \times 10^{-6}\ K^{-1}$ by Fink [35]).

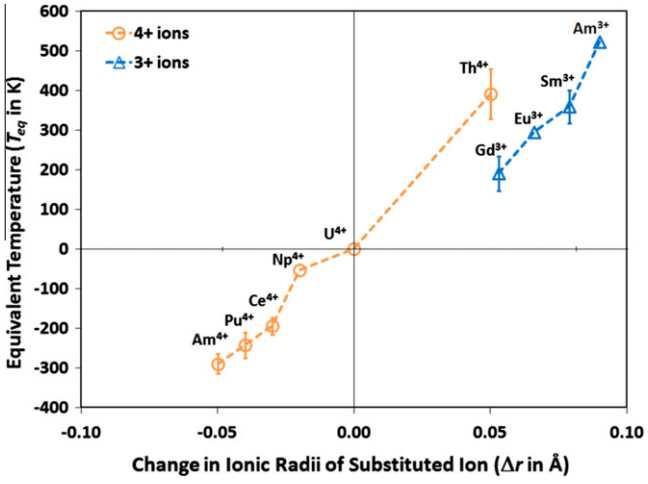

Fig. 10. The calculated equivalent temperature (T_{eq}) for each type of substituted specie in UO_2 to achieve an equal amount of lattice expansion or contraction in a perfect UO_2 lattice. The experimental linear thermal expansion coefficient was used to derive these temperatures. The error bars are associated with the predicted T_{eq} with different potentials for a particular substituted ion.

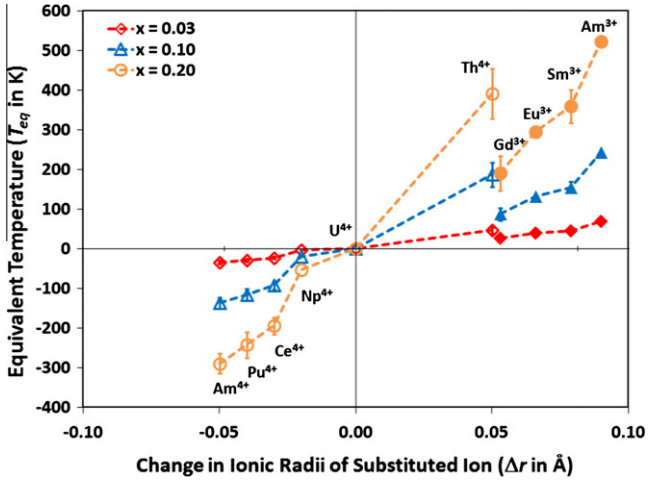

Fig. 11. The effect of concentration on the equivalent temperature (T_{eq}) for each type of substituted specie in UO_2. The open symbols are for 4+ ions and solid symbols are for 3+ ions. The magnitude of T_{eq} increases with an increase in concentration. The error bars are associated with the predicted T_{eq} for a particular substituted ion with different potentials.

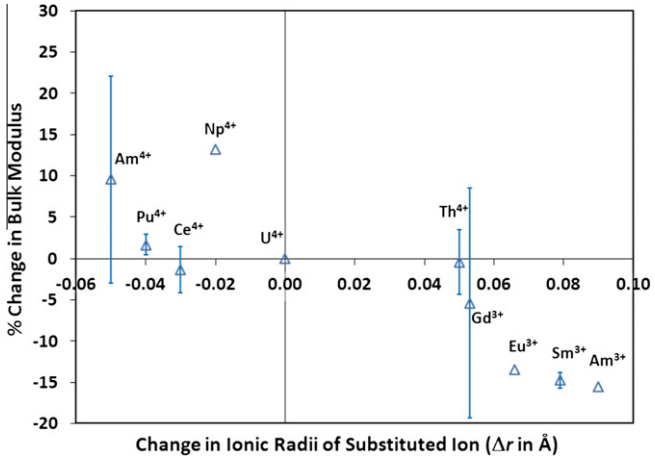

Fig. 12. The % change in bulk modulus calculated for each type of substituted specie in UO_2. Most of the 4+ ions increase the bulk modulus while most of the 3+ ions reduce the bulk modulus. The error bars are associated with the predicted % change in bulk modulus with different potentials for a particular substituted ion.

sion for Am^{3+} is equivalent to increasing the temperature by ~520 K in pure UO_2. The deviation between 4+ and 3+ ions are observed between Th^{4+} ($\Delta r = +0.050$ Å) and Gd^{3+} ($\Delta r = +0.053$ Å). The equivalent temperatures are estimated to be +391 K and +221 K for Th^{4+} and Gd^{3+} respectively. We also estimated the effect of concentration on the equivalent temperatures. Fig. 11 illustrates the variation in equivalent temperatures for three different concentrations ($x \sim 0.03$, 0.10, and 0.20). The absolute magnitudes of the equivalent temperatures increase with an increase in the concentration of the substituted ions.

Fig. 12 shows the effect of substitution on bulk modulus. Most of the 4+ ions increase the bulk modulus of the urania matrix, which can be explained by the decrease in lattice parameter for 4+ ion substitution. Similarly most of the 3+ ions decrease the bulk modulus. For example, if we consider 20% substitution in UO_2 matrix, Am^{3+} reduces the bulk modulus by ~16%.

The incorporation of Lanthanides and Actinides in the urania matrix affects various thermo-physical properties such as elastic properties, thermal conductivity, ionic diffusion, phase stability. In this manuscript we have investigated the effect of Lanthanide and Actinide substitution in UO_2 matrix. We defined chemical expansion and the chemical expansion coefficient that relates the change in lattice parameter with ionic substitution. We then used this parameter to estimate the effect of 3+ and 4+ Lanthanide and Actinide substitution in the UO_2 matrix. The results show that the structural and elastic properties are dependent on the elastic and electrostatic effects. Elastic effects are prominent for 4+ ion substitution, while both elastic and electrostatic effects are important for 3+ ion substitution. Further it is seen that all the ions with smaller ionic radii than the U^{4+} ions reduce the lattice parameter, while ions with larger ionic radii than the U^{4+} ions increase the lattice parameter. The chemical expansions due to substitution are used to estimate the equivalent temperature required to obtain similar lattice variation in pure UO_2. This study provides atomic level understanding of the effect of substitution on elastic properties of the urania fuel and is useful for understanding the effect of fission products on UO_2 properties, on the properties of mixed oxide fuels, and minor Actinide based fuels used for reprocessing.

Acknowledgements

This work was funded by DOE-NEUP DE-AC07-05ID14517 and NRC Faculty Development Grant.

References

[1] H. Kleykamp, J. Nucl. Mater. 131 (1985) 221–246.
[2] J.R. Lamarsh, A.J. Baratta, Introduction to Nuclear Engineering, third ed., Prentice Hall, 2001.
[3] J.K. Shultis, R.E. Faw, Fundamentals of Nuclear Science and Engineering, second ed., CRC Press, 2007.
[4] D.R. Olander, Fundamental Aspects of Nuclear Reactor Fuel Elements. Technical Information Center, Office of Public Affairs, Energy Research and Development Administration, 1976.
[5] M. Stan, Mater. Today 12 (2009) 20–28.
[6] V.V. Rondinella, T. Wiss, Mater. Today 13 (2010) 24–32.
[7] Status and Advances in MOX Fuel Technology, International Atomic Energy Agency, Technical Reports Secies No. 415, 2003.
[8] Thorium Fuel Cycle – Potential Benefits and Challenges, International Atomic Energy Agency, IAEA-TECDOC-1450, 2005.
[9] Status of minor actinide fuel development, International Atomic Energy Agency, NF-T-4.6, 2009.
[10] D.J. Kim, Y.W. Lee, Y.S. Kim, J. Nucl. Mater. 342 (2005) 192–196.
[11] V.I. Anisimov, J. Zaanen, O.K. Andersen, Phys. Rev. B 44 (1991) 943–954.
[12] V.I. Anisimov, F. Aryasetiawan, A.I. Lichtenstein, J. Phys. – Condens. Matter 9 (1997) 767–808.
[13] J.G. Yu, R. Devanathan, W.J. Weber, J. Phys. – Condens. Matter. 21 (2009) 435401.
[14] S.C. Middleburgh, D.C. Parfitt, R.W. Grimes, B. Dorado, M. Bertolus, P.R. Blair, L. Hallstadius, K. Backman, J. Nucl. Mater. 420 (2012) 258–261.
[15] R.W. Grimes, C.R.A. Catlow, Philos. Trans. Roy. Soc. – Math. Phys. Eng. Sci. 335 (1991) 609–634.
[16] R.W. Grimes, G. Busker, Nucl. Energy – J. Br. Nucl. Energy Soc. 35 (1996) 403–410.
[17] A.R. Cleave, Atomic scale simulations for waste form applications, Ph.D. thesis, Advised by R.W. Grimes, Department of Materials, Imperial College, London, 2006.
[18] M. Nadeem, M.J. Akhtar, R. Shaheen, M.N. Haque, A.Y. Khan, J. Mater. Sci. Technol. 17 (2001) 638–642.
[19] M. Osaka, J. Adachi, K. Kurosaki, M. Uno, S. Yamanaka, J. Nucl. Sci. Technol. 44 (2007) 1543–1549.
[20] T. Uchida, T. Arima, K. Idemitsu, Y. Inagaki, Comput. Mater. Sci. 45 (2009) 229–234.
[21] T. Arima, S. Yamasaki, Y. Inagaki, K. Idemitsu, J. Alloys Compd. 400 (2005) 43–50.
[22] B.G. Dick, A.W. Overhauser, Phys. Rev. 112 (1958) 90–103.
[23] R.A. Buckingham, Proc. R. Soc. Lond. Ser. A 168 (1938) 264–283.
[24] P.M. Morse, Review 34 (1929) 57–64.
[25] J.D. Gale, J. Chem. Soc., Faraday Trans. 93 (1997) 629–637.
[26] J.D. Gale, A.L. Rohl, Mol. Simul. 29 (2003) 291–341.
[27] H. Xu, R.K. Behera, Y. Wang, F. Ebrahimi, S.B. Sinnott, E.D. Wachsman, S.R. Phillpot, Solid State Ionics 181 (2010) 551–556.
[28] J. von Pezold, A. Dick, M. Friak, J. Neugebauer, Phys. Rev. B 81 (2010) 094203.
[29] R.D. Shannon, C.T. Prewitt, Acta Crystallogr. Sect. B – Struct. Crystallogr. Cryst. Chem. B 25 (1969) 925–946.
[30] K. Govers, S. Lemehov, M. Hou, M. Verwerft, J. Nucl. Mater. 366 (2007) 161–177.
[31] K. Govers, S. Lemehov, M. Hou, M. Verwerft, J. Nucl. Mater. 376 (2008) 66–77.
[32] J. Belle, R.M. Berman, Thorium Dioxide: Properties and Nuclear Applications, United States Department of, Energy, DOE/NE0060, 1984.
[33] D.J. Green, An Introduction to the Mechanical Properties of Ceramics, Cambridge University Press, 2004.
[34] S. McIntosh, J.F. Vente, W.G. Haije, D.H.A. Blank, H.J.M. Bouwmeester, Chem. Mater. 18 (2006) 2187–2193.
[35] J.K. Fink, J. Nucl. Mater. 279 (2000) 1–18.
[36] R.K. Behera, C.S. Deo, Effect of Ce^{4+} and Th^{4+} Ion Substitution in Uranium Dioxide, in: MRS Proceedings 1383, mrsf11-1383-a01-03, 2012 <http://dx.doi.org/10.1557/opl.2012.1240>.